Attribute-driven footprint suppression

Scott Falconer, University of Houston; Kurt J. Marfurt, The University of Oklahoma*

ABSTRACT

Most land seismic data volumes suffer from acquisition footprint which can often be confused with faults, fractures, and karst. Geometric attributes such as coherence and curvature enhance the appearance of subtle geologic features, but also exacerbate footprint artifacts. We use this 'negative' feature of geometric attributes as a means of characterizing short-wavelength footprint components. Once characterized, we subtract the footprint from the migrated seismic data volume using an adaptive subtraction technique and recompute attributes from these filtered data volumes. We demonstrate the effectiveness and pitfalls of this approach on a data volume exhibiting karst from the Central Basin Platform of west Texas,

INTRODUCTION

Seismic data are plagued with various kinds of noise. While there are a wide array of preprocessing steps to suppress the noise before the data are stacked these steps are not perfect such that some noise will always contaminate our data. One such type of noise is acquisition footprint. Marfurt et al. (1998) define acquisition footprint as "any pattern of noise that is highly correlated to the geometric distribution of sources and receivers on the earth's surface." Causes of acquisition footprint include inaccurate velocity models, inaccurate statics, migration operator aliasing, leakage of aliased coherent noise (i.e. surface waves), irregular patterns of varying fold and azimuthal distribution, and incomplete data due to obstacles.

Acquisition footprint is vexing to interpreters since it can be confused on time slices with faults, fractures, and karst features of geologic interest. Avoiding acquisition footprint is nearly impossible with 3D data due to suboptimal acquisition geometries arising from limited exploration budgets and limited field access.

Seismic attributes allow interpreters to extract subtle geologic features in the seismic data that may otherwise be difficult to see. Unfortunately, some of these geologic features have forms that appear similar to acquisition footprint. As an example, the objective in Figure 1a is to map subtle karst features at the San Andres level that may form an updip seal for oil production to the east. If we look at a slightly shallower time slice in Figure 1b, we note that the 'karst' features at the San Andres level may actually be a footprint artifact. In general, small defects in the seismic data will be exacerbated by seismic attributes. Attributes such as coherence are sensitive to lateral changes in wave form. Attributes such as the Sobel filter edge detector (Luo et al., 1996), the generalized Hilbert transform (Luo et al., 2004), and coherent amplitude gradients (Marfurt, 2006) are sensitive to lateral changes in amplitude along a dipping reflector. Curvature (al Dossary and Marfurt, 2006) is sensitive to lateral changes in reflector dip.

Different acquisition and processing errors can give rise to changes in waveform, amplitude, and dip (Hill, 1999). Migration and DMO artifacts due to data and/or operator aliasing give rise to organized ellipses that result in changes in both amplitude and apparent dip. Systematic errors in velocity analysis can also give rise to organized 'acquisition footprint' (Hedke et al., 2007). In general, attributes are sensitive to relatively short wavelength components of acquisition footprint, making attributes an excellent tool in footprint characterization.

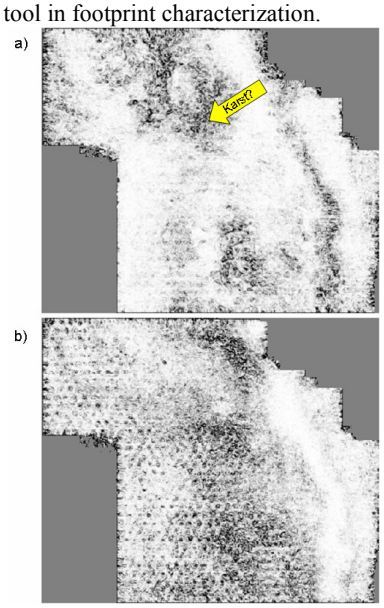

Figure 1. (a) Time slice at t = 0.6 s through a generalized Sobel filter edge detection algorithm that delineates 'karst' in the San Andres formation. (b) The time slice at t = 0.5 s shows that these 'karst' features may actually be acquisition footprint. (Original seismic data courtesy of Burlington Resources).

Several remedies used to suppress acquisition footprint have involved time slices. Gulunay et al. (1994), Gulunay (2000), and Soubaras (2002) both predicted the pattern of acquisition footprint from the surface recording geometry

assuming flat reflectors. Gulunay designed k_x-k_y wavenumber notch filters to suppress the predicted footprint and applied them to the k_x-k_y components of the seismic time slices. Soubaras modified this approach by designing a spatial *f(x,y)* adaptive filter to subtract the predicted footprint pattern.

Chopra and Larsen (2000) noted that volumetric coherence exacerbated acquisition footprint such that it can be used to better characterize its k_x-k_y spectrum. k_x-k_y notch filters designed on the attributes were then applied to the seismic amplitude time slices. Drummond et al. (2000) determined the footprint pattern by examining k_x-k_y spectra of the seismic data time slices. After transforming the k_x-k_y noise components back to *x*-*y* space, they applied an adaptive filter to subtract the estimated noise from the original, unfiltered time slice. Unfortunately, they do not describe how they chose their k_x-k_y components, nor how they implemented their adaptive filter.

Cvetkovic et al. (2007) attacked acquisition footprint using 2D stationary wavelet transforms applied to time slices. The interpreter identifies and determines amplitude cutoffs for wavelet components (or scales) that represent the footprint on a coarse grid of time slices. Those components that exceed the amplitude threshold are suppressed. Jervis (2006) used complex wavelets to suppress acquisition footprint although details of his implementation are not presented.

Acquisition footprint is often characterized by periodic artifacts correlated with the (periodic) acquisition geometry. Acquisition footprint in seismic and attribute time slices are generally worse in the shallow sections where we have the lowest fold, greatest variation in moveout, and thus most sensitivity to inaccurate velocities; footprint generally heal with depth. Geometric attributes are particularly sensitive to the short wavelength component of acquisition footprint and thus serve as a tool for its detection. Key to any k_x-k_y noise removal workflow is characterization of its spectrum.

Acquisition footprint enhancement

In order to suppress footprint we need to first recognize and characterize its behavior. Counter-intuitively, the first step in the suppression of acquisition footprint is to *enhance* it. Not only are seismic 'geometric' attributes such as coherence and curvature particularly sensitive to acquisition footprint, they are also computed along structural dip, and are thus relatively insensitive to changes in the waveform normally seen on horizontal time slices through amplitude data. For the artifacts in this survey, we find that the fractional derivative modification of the well-known Sobel filter used in photographic edge enhancement provides an excellent image of the footprint pattern .

Seismic attributes show more than faults, footprint, and channel edges. Chopra and Marfurt (2007) describe a rich suite of depositional and diagenetic features that can be delineated including mass transport complexes, levee-overbank complexes, bars, karst, and angular unconformities. Such features are often stratigraphically controlled and do not continue vertically above or below a temporally-delineated geologic formation. Following workflows developed for fault enhancement (e.g. Barnes, 2007) we apply a simple vertical running-window median filter to our attribute volumes to eliminate stratigraphic features and enhance vertical footprint. Attribute anomalies associated with stratigraphically-limited geological features will be suppressed while vertical footprint (and faults) will be preserved. We also use tapers to minimize k_x-k_y artifacts associated with the survey edges and no-permit areas.

Since common acquisition geometry programs use a regular and or staggered grid of shot lines and receiver lines, we anticipate that acquisition footprint will be spatially periodic. Figure 2 shows the periodicity of the footprint (yellow arrows).

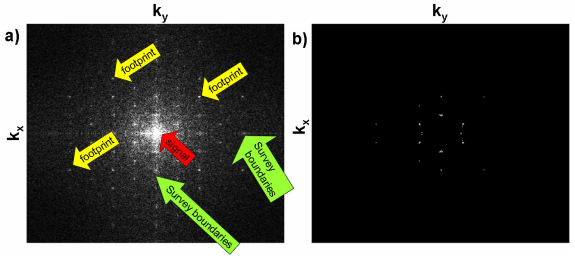

Figure 2. (a) k_x-k_y transform of the attribute slice shown in Figure 1b at t = 0.5 s. Yellow arrows indicate acquisition footprint with a periodicity of approximately 1.2 cycles/km in *x* and 1.5 cycles/km in *y*. The red center arrow indicates diffuse signal which lies within a circle of radius k_{max}= 0.2 cycles/km. The green arrows point to the survey boundaries on the k_x and k_y axis. (b) The mask generated from (a) using a threshold of 10 times the L1 norm of the amplitude spectrum.

Most of the geologic features (or signal) appears as an unorganized cloud centered about (k_x=0, k_y=0). The spectrum of discrete geologic discontinuities such as meandering channels, karst, and curvilinear faults, will be spread throughout the entire k_x-k_y spectrum. If we attempt to suppress footprint by muting values of $(k_x^2+k_y^2)>k_{max}^2$, we would smear, or perhaps even eliminate features of geologic interest . Once the nature of the footprint noise is determined, a mask is generated to pass the high-amplitude k_x-k_y components, with no mask filters applied within a circular exclusion region $(k_x^2+k_y^2) < k_{max}^2$. We find that semi-automatic detection of this mask can be achieved by setting an amplitude threshold value above the L1-norm of the k_x-k_y data. Quality control of the mute is perhaps the most important step in the whole process. To do so, we

pass rather than reject those k_x-k_y components of the original seismic amplitude time slice described by the mask and transform back to x-y space. Ideally, only the acquisition footprint and no geologic signal should show up on the reverse transformed slice. Experimenting with different values for the exclusion circle and threshold is the key to designing the optimal notch mute.

Once the masks are generated and quality controlled, the filter is ready to be applied to the original seismic data. The entire seismic data volume is sliced and k_x-k_y transformed into the wavenumber domain. The masks are applied and the result transformed back to x-y to generate slices of the modeled footprint (Figure 4a). In the ideal situation, the modeled footprint can be directly subtracted from the original seismic data. However, we expect there to be lateral changes in the acquisition geometry due to limited access or operational convenience. Equally common, we may wish to attack acquisition footprint seen on a merged survey where the acquisition geometry changes significantly from one part of the merged survey to another part. In the wavenumber domain, lateral shifts in a portion of the acquisition geometry will modulate the notches and smear them out. We therefore anticipate that we will need to do more than simple subtraction of any modeled noise from the original seismic amplitude data, but rather to adaptively subtract the noise from the signal.

ADAPTIVE SUBTRACTION

Adaptive subtraction is a technique that has gained significant popularity in long-period multiple suppression (Abma et al., 2005) and for our application requires only the sliced original seismic data, $d_{ij,}$ and the noise volume, n_{ij} estimated using a k_x-k_y , SVD, or other appropriate filter. The goal of the algorithm is to minimize the error between the original data, and a weighted version of the noise:

$$\min \varepsilon^2 = \sum_{k=1}^{K} \left(\sum_{j=-M_y}^{M_y} \sum_{i=-M_x}^{M_x} d_{l(k)+i,m(k)+j} - \alpha_k w_{i,j} n_{l(k)+i,m(k)+j} \right)^2 \quad , \qquad (1)$$

where ε is the error,
$d_{l(k)+i,m(k)+j}$ is the k^{th} windowed version of the original seismic data,
$n_{l(k)+i,m(k)+j}$ is the k^{th} windowed version of the noise,
$w_{ij}(x,y)$ is a 2D weighting function described in Figure 3, and
α_k is the amplitude of the k^{th} control point.
Minimizing equation 1 with respect to α_k, we obtain (in matrix form):

$$(\mathbf{wn})^{\mathrm{T}}(\mathbf{wn})\boldsymbol{\alpha} = (\mathbf{wn})^{\mathrm{T}}\mathbf{d} \quad , \qquad (2)$$

where **wn** is the windowed noise, and **α** are the control point amplitudes. Solving for the vector **α**, we obtain

$$\boldsymbol{\alpha} = \left[(\mathbf{wn})^{\mathrm{T}}(\mathbf{wn}) + \beta\mathbf{I}\right]^{-1}(\mathbf{wn})^{\mathrm{T}}\mathbf{d} \quad , \qquad (3)$$

where the small prewhitening factor , β, together with the identity matrix, **I**, prevents division by zero in dead-trace areas.

RESULTS

Figure 4c shows the weights computed using equation 3. These weights multiply the noise in Figure 4a to produce the noise in Figure 4b that better fits the original data. Finally the adaptive noise in Figure 4b is subtracted from the original seismic time slice shown in Figure 5a. Note that the generated weights may vary beyond 0 and 1 and are zero outside the survey boundaries. Ideally the weight values should be somewhere near one and not subtract the geologic signal. Negative weight values will add portions of the estimated noise to the data rather than subtract it.

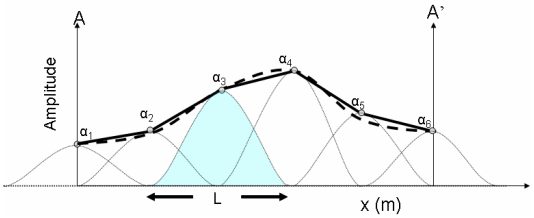

Figure 3. Representation of a 1D continuous function (dashed line) in the interval AA' using a suite of overlapping squared cosine basis functions. Each basis function has numerical support over a distance L. The 3rd basis function is shaded in blue. By fitting the amplitude of the control points α_k to least-squares fit the continuous curve, we obtain the smooth approximation shown above (solid line).

Blue arrows denote acquisition footprint on the original time slice at t = 0.5 s shown in Figure 5a. We show the k_x-k_y filtered seismic data without adaptive subtraction in Figure 5b. Note that noise is subtracted even in the dead trace areas. Figure 5c is the adaptive subtraction filtered time slice.

To quality control this process we recompute the footprint-sensitive seismic attributes from the adaptive-subtraction-filtered seismic data volume. Figure 6a shows a generalized Sobel filter time slice at the San Andres level at t = 0.6 s. Blue arrows indicate acquisition footprint. Figure 6b shows the attribute volume calculated by subtracting the k_x-k_y predicted noise from the original seismic data . While the erroneous noise in the dead trace zone is small, it makes us question whether the raw k_x-k_y predicted noise is an overall good fit to the data. Figure 6c shows the Sobel filter derived from the adaptive subtraction filtered seismic data. . We note that many of the footprint artifacts are now eliminated.

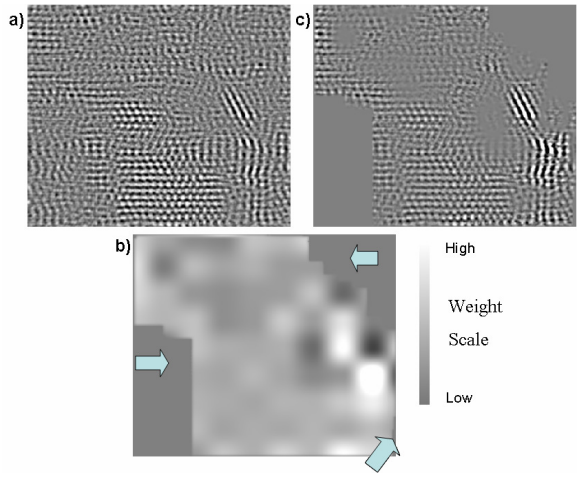

Figure 4. Time slices through volumes at $t = 0.5$ s: (a) noise corresponding to the k_x-k_y mask applied to the transformed seismic data, (b) weights computed using equations 1-3, and (c) weighted noise using the adaptive subtraction algorithm. Notice that the generated weights outline the survey area and the area of dead traces denoted by the blue arrows is properly assigned weight values of zero. If the values of all the weights were 1.0 then (a) and (c) would be identical.

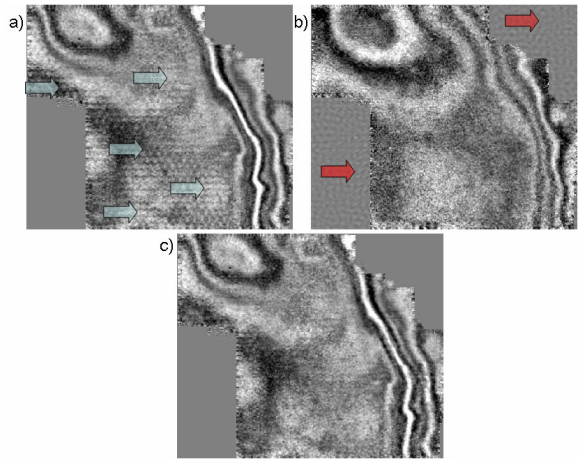

Figure 5. (a) Seismic time slice at $t = 0.5$ s through the migrated data volume. Blue arrows indicate acquisition footprint. (b) k_x-k_y filtered time slice where the predicted noise shown in Figure 4a is simply subtracted from (a). Magenta arrows indicate artifacts introduced outside the survey boundary. (c) The filtered data after adaptive subtraction.

CONCLUSIONS

We present a post-migration footprint suppression workflow that is ideally implemented by the seismic interpreter. The seismic interpreter chooses seismic attributes that are sensitive to a footprint component of interest and then designs footprint-suppression filters.

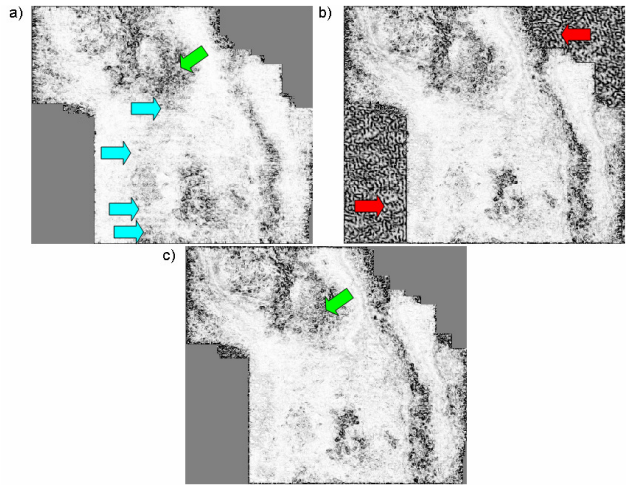

Figure 6. Time slices at t =0 .6 s at the San Andres level through the generalized Sobel filter volumes computed from (a) the original data, and from k_x-k_y filtered data (b) without and (c) with adaptive subtraction. Blue arrows indicate acquisition footprint. Magenta arrows indicate artifacts in the dead trace zone. We now feel confident in identifying the anomaly indicated by the green arrow as karst.

We find k_x-k_y noise prediction designed from attribute time slices followed by an adaptive subtraction filter suppresses footprint and removes a minimal amount of signal. Lack of care in selecting the k_x-k_y results in removing signal. Vertical slices through the rejected seismic noise show both incoherent noise and organized reflections, with the latter predicted by Hill (1999). By construction, this workflow does not reject long-wavelength components of footprint which could adversely impact impedance inversion and subsequent processes.

ACKNOWLEDGEMENTS

The authors would like to thank Burlington Resources for the use of their seismic data volumes. This work was partially supported by a U.S. DOE project entitled ‘‘Improving geologic and engineering models of Midcontinent fracture and karst-modified reservoirs using 3D seismic attributes’. Siva Nagarajan, Hao Guo, Felipe Lozano, helped in programming and attribute computation.